nature biotechnology

RESOURCE

Systematic exploration of essential yeast gene function with temperature-sensitive mutants

Zhijian Li[1,8], Franco J Vizeacoumar[1,8], Sondra Bahr[1], Jingjing Li[1], Jonas Warringer[2], Frederick S Vizeacoumar[3], Renqiang Min[1], Benjamin VanderSluis[4], Jeremy Bellay[4], Michael DeVit[5], James A Fleming[5], Andrew Stephens[6], Julian Haase[6], Zhen-Yuan Lin[1], Anastasia Baryshnikova[1], Hong Lu[1], Zhun Yan[1], Ke Jin[1], Sarah Barker[1], Alessandro Datti[3,7], Guri Giaever[1], Corey Nislow[1], Chris Bulawa[5], Chad L Myers[4], Michael Costanzo[1], Anne-Claude Gingras[1], Zhaolei Zhang[1], Anders Blomberg[2], Kerry Bloom[6], Brenda Andrews[1] & Charles Boone[1]

Conditional temperature-sensitive (ts) mutations are valuable reagents for studying essential genes in the yeast *Saccharomyces cerevisiae*. We constructed 787 ts strains, covering 497 (~45%) of the 1,101 essential yeast genes, with ~30% of the genes represented by multiple alleles. All of the alleles are integrated into their native genomic locus in the S288C common reference strain and are linked to a *kanMX* selectable marker, allowing further genetic manipulation by synthetic genetic array (SGA)–based, high-throughput methods. We show two such manipulations: barcoding of 440 strains, which enables chemical-genetic suppression analysis, and the construction of arrays of strains carrying different fluorescent markers of subcellular structure, which enables quantitative analysis of phenotypes using high-content screening. Quantitative analysis of a GFP-tubulin marker identified roles for cohesin and condensin genes in spindle disassembly. This mutant collection should facilitate a wide range of systematic studies aimed at understanding the functions of essential genes.

© 2011 Nature America, Inc. All rights reserved.

The budding yeast *S. cerevisiae* is one of the most well-characterized model organisms for systematic analysis of fundamental eukaryotic processes. Approximately 19% of *S. cerevisiae* genes are considered essential, because haploid spores carrying a deletion allele of these genes fail to germinate and form colonies under standard laboratory conditions[1]. Comparative analysis revealed that gene dispensability is highly conserved (~83%) between *S. cerevisiae* and the distantly related yeast species, *Schizosaccharomyces pombe,* supporting the presence of strong selective pressure to retain essential gene activity across large evolutionary distances[2]. Indeed, essential genes tend to be more highly conserved from yeast to humans when compared to nonessential genes[3]. The set of essential yeast genes spans diverse biological processes and although the primary role of most essential yeast genes has been characterized, the full breadth of function associated with essential genes has not been examined, owing, at least in part, to the lack of adequate genetic reagents for their conditional and systematic perturbation. Here we present the construction and characterization of an extensive set of conditional ts alleles of *S. cerevisiae* essential genes. Other types of mutant alleles that perturb essential gene functions include cold-sensitive[4], temperature-inducible degron[5], tetracycline-regulatable promoter-replacement[6] and decreased abundance by mRNA perturbation alleles[7]. However, ts alleles often provide the simplest and most finely tuned control of gene function, enabling permissive, semi-permissive and restrictive conditions to be established easily. At the permissive temperature, the phenotype of a ts mutant resembles that of the wild-type strain, whereas at the restrictive temperature, the activity of the essential gene is substantially reduced or abolished, resulting in a slow-growth or lethal phenotype. We collected hundreds of previously characterized ts alleles as yeast mutants or DNA clones from the yeast community and then amplified by PCR the ts alleles and integrated them at their native locus in the reference (S288c) genetic background, generating a set of 787 ts mutants spanning 497 different essential genes that are isogenic except for the ts allele we introduced. Our new set expands upon a nonoverlapping set of 250 ts strains constructed recently[8], which combined cover ~65% of *S. cerevisiae* essential genes.

In this study, we characterize the ts mutant array as a resource for exploring the pleiotropic roles of highly conserved essential pathways in yeast using high-resolution growth profiling, chemical-genetic suppression and high content screening (HCS) experiments. The HCS experiments involved quantitative single-cell image analysis of fluorescent markers for specific pathways and structures in hundreds of different ts mutants. Our results highlight a role for two essential protein complexes, cohesin and condensin, in mitotic spindle disassembly.

[1]Banting and Best Department of Medical Research and Department of Molecular Genetics, The Donnelly Centre, University of Toronto, Toronto, Ontario, Canada. [2]Department of Cell and Molecular Biology, Göteborg University, Göteborg, Sweden. [3]Samuel Lunenfeld Research Institute, Mount Sinai Hospital, Toronto, Ontario, Canada. [4]Department of Computer Science and Engineering, University of Minnesota, Minneapolis, Minnesota, USA. [5]FoldRx Pharmaceuticals Inc., Cambridge, Massachusetts, USA. [6]Department of Biology, University of North Carolina, Chapel Hill, North Carolina, USA. [7]Department of Experimental Medicine and Biochemical Sciences, University of Perugia, Perugia, Italy. [8]These authors contributed equally to this work. Correspondence should be addressed to B.A. (brenda.andrews@utoronto.ca) or C.B. (charlie.boone@utoronto.ca).

Received 13 January; accepted 1 March; published online 27 March 2011; doi:10.1038/nbt.1832

RESULTS

Construction and confirmation of ts yeast strains

We collected hundreds of previously characterized yeast strains and DNA constructs carrying ts alleles and integrated the conditional alleles into the S288c reference background[9]. In total, we constructed a set of 787 ts strains representing 497 different essential genes or ~45% of the essential gene set (**Supplementary Table 1**), which covers a representative proportion of Gene Ontology (GO) molecular functions and biological processes for the complete essential gene set. Each ts allele was integrated into its native locus such that it was linked to a kanamycin-resistant cassette, *kanMX*, which was targeted to the 3′ UTR region of the gene and placed 0–300 bp downstream of the stop codon (**Supplementary Table 2**). We designed the integration such that the intervening sequences were not altered to avoid perturbing the expression of neighboring genes (**Supplementary Fig. 1**). Two PCR reactions were carried out to confirm that: (i) the *kanMX* cassette was linked to the expected target gene, and (ii) the *kanMX* cassette integrated at the expected genomic location (**Supplementary Fig. 1**). Correct integration was confirmed for all of 787 ts alleles using this PCR-based strategy (**Supplementary Table 1**).

The ts strain collection was further validated by plasmid complementation. Individual plasmids encoding wild-type genes corresponding to 786 of 787 alleles in the ts collection were taken from either the low-copy, molecular barcoded yeast open reading frame (MoBY-ORF) library[10] or the high-copy yeast genomic tiling collection[11] (neither library contained a plasmid encoding *CDC39*), transformed into the corresponding ts mutant strain and subsequently grown at permissive and restrictive temperatures. We observed plasmid-dependent rescue for 782 of 786 strains representing 494 essential genes in our collection, confirming that the expected allele was responsible for the growth phenotype (**Supplementary Table 1**). In summary, 782 of 787 ts strains representing 494 essential genes were confirmed by both PCR and plasmid complementation.

Profiling the temperature sensitivity of ts alleles

We next applied high-resolution growth profiling to characterize the temperature sensitivity of mutants in our strain collection. Lag time, growth rate and growth efficiency were quantified across a range of temperatures to generate a growth profile for each ts mutant (**Fig. 1a** and **Supplementary Table 3**). The reference strain BY4741 reached its maximal growth rate at 32–36 °C, whereas growth efficiency and growth lag continuously decreased from a maximum at 24 °C (**Supplementary Fig. 2a**). Individual ts-strain growth profiles were normalized against a reference wild-type profile to provide a measure of relative growth defects at each temperature. As expected, the frequency distribution of relative growth rates reflected the tendency toward exaggerated growth defects at higher temperatures (**Supplementary Fig. 2b**). In addition, after normalizing for defects at 22 °C, we found that the fraction of ts strains with clear temperature-dependent growth defects expanded with increasing temperature, from 24 °C to 34 °C (**Fig. 1b**).

Notably, comparison of average pair-wise Pearson correlation coefficients revealed that ts alleles corresponding to the same gene tended to show more similar temperature profiles than alleles of different essential genes ($P = 10^{-23}$) (**Supplementary Fig. 2c**), suggesting that the ts-strain growth profiles may reflect essential gene function. Moreover, ts alleles of essential genes that participate in the same cellular process also tend to show more similar temperature profiles than essential gene alleles that do not share a similar function (comparison of average pair-wise Pearson correlation coefficients, excluding within-gene comparisons, $P = 10^{-83}$), thus further supporting a relationship between ts-strain growth profiles and protein function. Consistent with this trend, hierarchical clustering of liquid growth profiles revealed that ts mutations in functionally related genes showed similar growth behavior in response to temperature (**Fig. 1c** and **Supplementary Fig. 2d**). Thus, the ts-strain growth profiles may represent distinct phenotypic fingerprints that reveal physiological defects associated with different essential cellular functions. However, we noted that whereas a general relationship between essential gene function and the ts-strain growth profile appears to exist, this trend may not hold true for all genes, especially those encoding multifunctional protein products involved in diverse cellular processes.

Chemical-genetic suppression analysis with a barcoded ts library

The ts mutant collection provides a reagent for performing systematic chemical-genetic suppression analysis. In this analysis, the ts mutants are grown in the presence of small-molecule compounds at both permissive and nonpermissive temperatures. Strains that grow at the

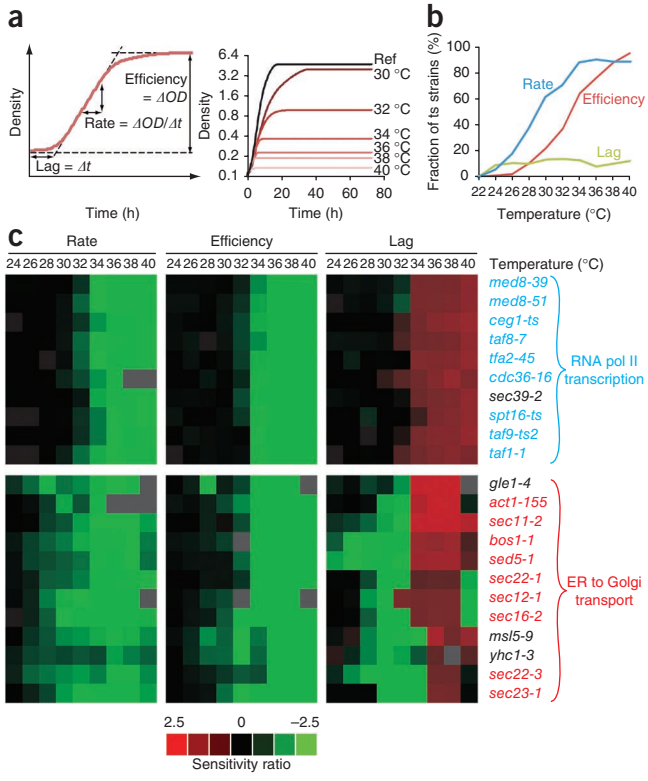

Figure 1 Profiling the temperature sensitivity of ts strains. (**a**) Left panel; general interpretation of high-resolution liquid growth profiles of strains harboring ts alleles. Growth rate (population doubling time) was determined by measuring the slope of the exponential phase of the growth curve. Lag was given by the intercept of the initial density and the slope, and growth efficiency was calculated as the total change in density for cells having reached stationary phase. Right panel; sample growth curves of the strains with the *act1-105* ts allele, obtained by microcultivation over a temperature range. (**b**) The fraction of all ts strains that exhibit significant ($P < 0.001$) temperature sensitive defects in growth rate (blue), lag (green) and/or efficiency (red) phases compared to wild type (WT) at the indicated temperatures. (**c**) Uncentered hierarchical clustering of ts allele growth profiles over all three growth variables. Profile similarity was measured using a Pearson similarity metric and average linkage mapping. The ts-strain sensitivity ratio is expressed as log2(WT/ts strain) at temperature X – log2(WT/ts strains) at 22 °C. ER, endoplasmic reticulum.

© 2011 Nature America, Inc. All rights reserved.

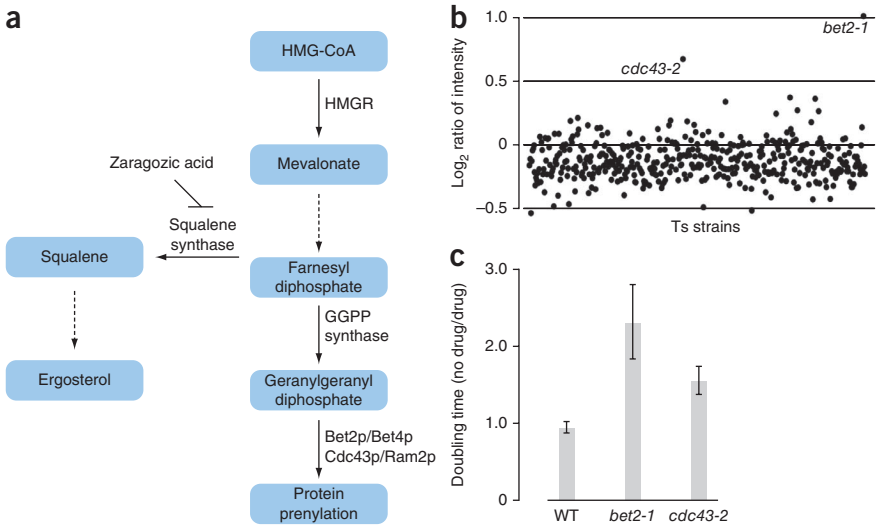

Figure 2 Zaragozic acid rescues *bet2-1* and *cdc43-2* ts phenotype. (**a**) Isoprenoid pathway in *S. cerevisiae*. The solid lines indicate one step and the dashed lines indicate multiple synthetic steps in the ergosterol and protein prenylation pathways[44–46]. (**b**) A pool of 440 barcoded ts mutants was grown in rich (YPD) medium in the presence of 4 mM of zaragozic acid A (ZA) or DMSO at 36.5 °C. Genomic DNA was prepared from cells after five generations of growth. Molecular barcodes were amplified by PCR and hybridized to a microarray (GeneChip Genflex Tag 16K Array v2, Affymetrix). The *x* axis represents the 440 ts strains ordered alphabetically by systematic name. The *y* axis represents the log2 ratio of barcode hybridization intensity between the ZA treatment and the solvent (DMSO) treatment. Mutants with highest log2 ratios at the restrictive temperature were identified as suppressors. (**c**) Yeast cells were grown in YPD with or without ZA in a 96-well plate at 36.5 °C. Fitness was defined as the ratio of doubling times measured in DMSO compared to ZA treatment. Error bars represent s.d. for four independent experiments.

© 2011 Nature America, Inc. All rights reserved.

nonpermissive temperature contain mutations that are suppressed by a particular compound. This contrasts with chemical-genetic sensitivity analysis that is often performed with the yeast deletion mutant collection, in which mutants are scored for growth sensitivity to a specific compound[12,13]. Notably, the use of suppression, rather than growth sensitivity, as a phenotype, enables screens for compounds that are not necessarily antifungals.

High-throughput chemical genetics of the deletion collection is possible because each strain contains two oligonucleotide molecular barcodes flanked by common primer sites. This enables mutants to be pooled, grown competitively in a single culture with a chemical and their relative fitnesses quantitatively estimated by measuring the abundance of each barcode in the culture using a microarray or sequencing[14–16]. To facilitate competitive growth assays using pools of ts mutant alleles, we applied the barcoder approach[17] to introduce molecular barcodes into a subset of ~400 ts strains such that the *HO* allele is replaced by a drug-resistance marker flanked by two unique oligonucleotides.

As a proof-of-principle analysis, we screened for mutations suppressed by zaragozic acid A (Squalestatin), an inhibitor of mammalian and fungal squalene synthase[18,19]. This is the first committed enzyme in sterol synthesis (**Fig. 2a**), and has received attention as a potential target for lipid-lowering agents[20]. We pooled the barcoded subset of ts strains, grew them at 36.5 °C in the presence or absence of zaragozic acid A and then quantified the molecular barcodes using barcode microarray analysis. Two strains, *bet2-1* and *cdc43-2*, were overrepresented in the pooled population exposed to zaragozic acid A, indicating that this compound suppressed ts growth defects associated with these mutant alleles (**Fig. 2b**). Suppression of *bet2-1* and *cdc43-2* growth defects was also confirmed by liquid growth assays and spot dilution assays on solid media (**Fig. 2c** and data not shown). *BET2* encodes the catalytic subunit of the type II geranylgeranyl transferase and *CDC43* encodes the beta subunit of geranylgeranyltransferase type I involved in prenylation (**Fig. 2a**). Previous studies have shown that when squalene synthase is inhibited by zaragozic acid A, intracellular levels of squalene and post-squalene metabolites are decreased, whereas the levels of other metabolites synthesized from the squalene precursor are increased, such as farnesyl diphosphate (FPP)[18] and farnesoic acid-derived metabolites[19]. Thus, zaragozic acid A may suppress the *bet2-1* and *cdc43-2* ts phenotype at restrictive temperature by increasing levels of cellular farnesyl diphosphate and geranylgeranyl diphosphate.

High-content screens to predict essential gene function

Having all of the ts alleles in an isogenic background allows the strain collection to be genetically modified using existing high-throughput strain manipulation methods, such as those developed to create double mutants for synthetic genetic array (SGA) analysis. Combining these manipulations with high-content screening enables functional discovery through the visualization and quantitative measurement of specific morphological features at a single-cell level[21]. We first constructed a panel of strains expressing fluorescent markers that represent six fundamental subcellular compartments or structures (**Fig. 3a**). Next, we crossed these reporters into an array of 762 ts strains (**Supplementary Table 1**) to create double mutants expressing a subcellular marker and a ts allele. Then, we imaged both the ts and the wild-type control strains at 26 °C and 32 °C. We chose 32 °C as a screening temperature because ~80% of the mutant alleles showed a growth defect at this temperature (**Fig. 1b**). We developed customized software[21] that automates image analysis and measures several morphological features, generating a quantitative and unique cell morphology profile for each ts mutant strain. The cell morphology profile comprises features such as cell shape, budding index, organelle density and 85 reporter-specific parameters (**Supplementary Table 4**). Notably, we confirmed all computationally derived phenotypes by visual inspection of the corresponding images (**Supplementary Table 5**), generating a high confidence and systematic profile for each ts strain. The raw morphometric data measured at both permissive and restrictive temperatures are provided in **Supplementary Table 6**.

In principle, a cell morphology profile should provide a rich phenotypic signature revealing functional relationships between genes. For example, mutants exhibiting increased DNA damage foci, as measured by Ddc2p-GFP localization, were enriched for essential genes involved in DNA replication ($P = 2.1 \times 10^{-10}$), prereplicative complex assembly ($P = 1.4 \times 10^{-5}$) and/or DNA synthesis during DNA repair ($P = 2.0 \times 10^{-5}$). The number of gene-specific profiles indicative of morphological defects increased at elevated temperature further

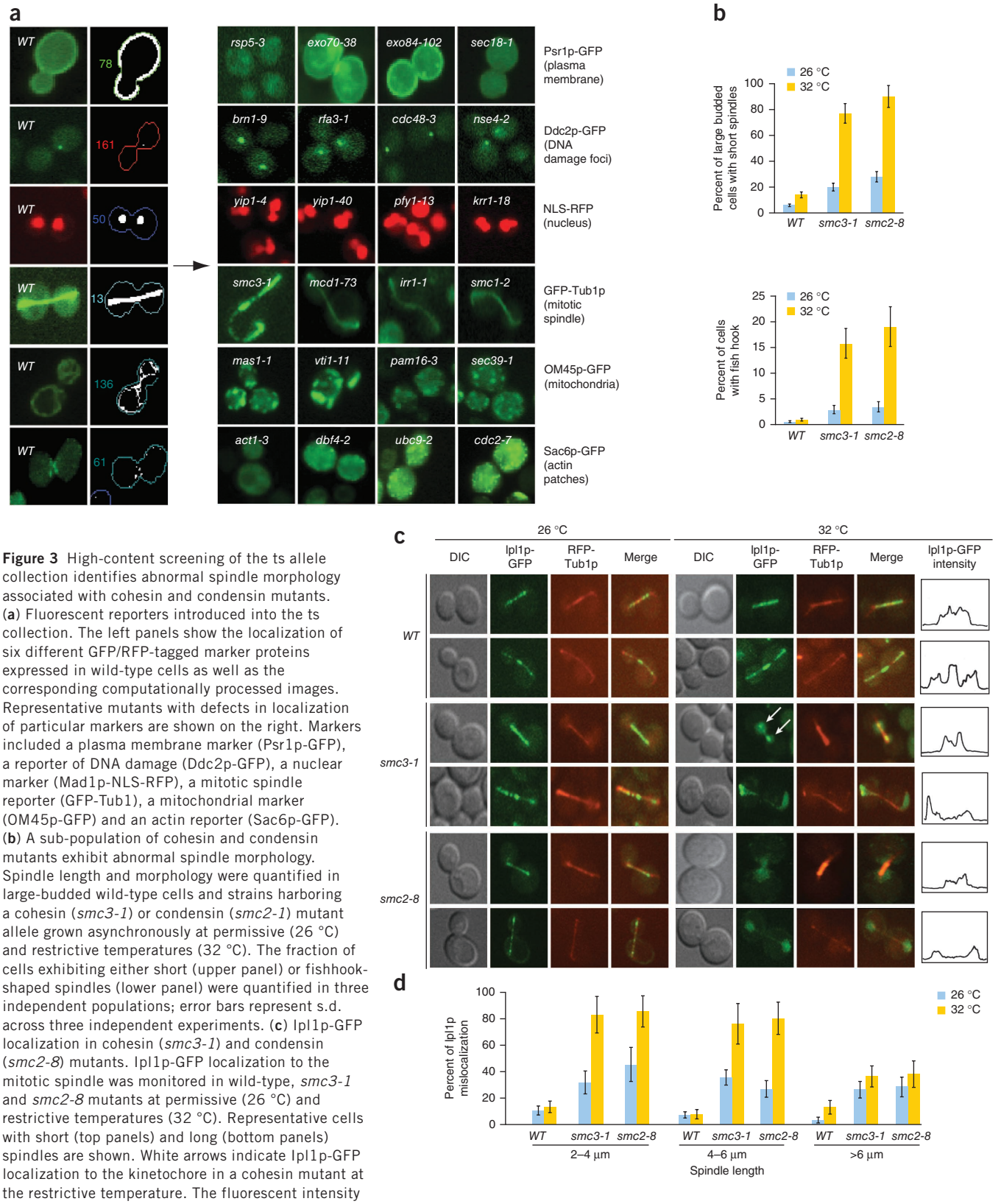

Figure 3 High-content screening of the ts allele collection identifies abnormal spindle morphology associated with cohesin and condensin mutants. (**a**) Fluorescent reporters introduced into the ts collection. The left panels show the localization of six different GFP/RFP-tagged marker proteins expressed in wild-type cells as well as the corresponding computationally processed images. Representative mutants with defects in localization of particular markers are shown on the right. Markers included a plasma membrane marker (Psr1p-GFP), a reporter of DNA damage (Ddc2p-GFP), a nuclear marker (Mad1p-NLS-RFP), a mitotic spindle reporter (GFP-Tub1), a mitochondrial marker (OM45p-GFP) and an actin reporter (Sac6p-GFP). (**b**) A sub-population of cohesin and condensin mutants exhibit abnormal spindle morphology. Spindle length and morphology were quantified in large-budded wild-type cells and strains harboring a cohesin (*smc3-1*) or condensin (*smc2-1*) mutant allele grown asynchronously at permissive (26 °C) and restrictive temperatures (32 °C). The fraction of cells exhibiting either short (upper panel) or fishhook-shaped spindles (lower panel) were quantified in three independent populations; error bars represent s.d. across three independent experiments. (**c**) Ipl1p-GFP localization in cohesin (*smc3-1*) and condensin (*smc2-8*) mutants. Ipl1p-GFP localization to the mitotic spindle was monitored in wild-type, *smc3-1* and *smc2-8* mutants at permissive (26 °C) and restrictive temperatures (32 °C). Representative cells with short (top panels) and long (bottom panels) spindles are shown. White arrows indicate Ipl1p-GFP localization to the kinetochore in a cohesin mutant at the restrictive temperature. The fluorescent intensity line profile of Ipl1p-GFP for a representative cell is also shown. (**d**) Wild-type and mutant cells were divided into three separate groups based on spindle length (2–4 µm, 4–6 µm, >6 µm) as measured by assessment of an RFP-Tub1p marker. The percentage of cells in each spindle length group that exhibited mis-localized Ipl1p-GFP was measured at permissive and restrictive temperatures. Error bars represent the s.d. across three independent experiments.

© 2011 Nature America, Inc. All rights reserved.

validated our approach (**Supplementary Fig. 3a**). We therefore developed a method to predict functional relationships based on the similarity of cell morphology profiles (**Supplementary Fig. 3b**,**c** and Online Methods).

Our computational classification approach identified known functional relationships between previously characterized essential genes. For example, mutants with known roles in mitochondrial protein import, such as *mas1-1* and *pam16-3*, exhibited defects in mitochondrial abundance whereas aberrant membrane targeting of the Psr1p-GFP reporter was observed in two exocyst mutants, *exo70-38* and *exo84-102* (**Fig. 3a**). Comparison of cell morphology profiles also uncovered gene-specific phenotypes, suggesting unanticipated functions for well-characterized essential genes. For example, components of cohesin, condensin and the chromosomal passenger complex (CPC), shared similar morphological profiles (**Fig. 3a** and **Supplementary Fig. 3c**). The products of *IPL1* (Aurora B kinase), *SLI15* (IN-CENP) and *BIR1* (SURVIVIN) interact to form the chromosomal passenger complex (CPC) that relocalizes dynamically in dividing cells to perform key mitotic roles[22–26]. Specifically, we found that cohesin mutants, including *smc3-1*, *mcd1-73*, *irr1-1* and *smc1-2* (**Fig. 3a**), as well as condensin mutants, *ycs4-1, smc2-8* and *smc4-1* (**Supplementary Table 5**) were characterized by a hyperelongated spindle phenotype with a 'fishhook' shape, as visualized using the tubulin marker GFP-Tub1p, suggesting that, similar to the CPC complex, cohesin and condensin may also be involved in spindle disassembly.

A role for cohesin and condensin in spindle disassembly

Because the regulation of spindle disassembly is not completely understood, we decided to further examine the potential role of cohesin and condensin in this essential process. Cohesins bind the sister chromatids together during metaphase and are cleaved in a separase-dependent fashion during anaphase[27,28]. When cells are synchronized in the G1 phase with α-factor and then released into the cell cycle at a restrictive temperature, ts cohesin mutants activate the mitotic checkpoint and arrest as large-budded cells with short or partially elongated spindles[29]. However, in our screen, when asynchronous cohesin ts mutants were shifted to restrictive temperature, we found two populations of cells: (i) large budded cells with short or partially elongated spindles, as expected, and (ii) a subpopulation of large budded cells with hyperelongated fishhook spindles, which presumably represent cells exhibiting a post-checkpoint spindle disassembly defect (**Fig. 3b**).

The fishhook spindle phenotype we observed may result from changes in microtubule[30] or CPC complex dynamics[21,22]. To examine this more carefully, we monitored spindle association and midzone enrichment of CPC components (Ipl1p-GFP, Sli15p-GFP and Bir1p-GFP) in a cohesin, *smc3-1*, and a condensin mutant, *smc2-8*. In wild-type cells, Ipl1p-GFP normally associates with short spindles ranging from ~1.5 to 2 μm in length, and this localization persists until the spindle disassembles, at which point Ipl1p localization is more prominent at the spindle midzone (**Fig. 3c**,**d**). Notably, in the cohesin mutants, Ipl1p-GFP, Sli15p-GFP and Bir1p-GFP associated with the kinetochore but failed to associate with the spindle until the spindle was >6 μm. In contrast, Ipl1p-GFP, Sli15p-GFP and Bir1p-GFP failed to localize to either the kinetochore or the spindle in condensin mutants (**Fig. 3c**,**d** and **Supplementary Fig. 4a**,**d**). Furthermore, the normal distribution of cohesin around the spindle, referred to as cohesin barrel, is lost in a *mcm21Δ* kinetochore mutant, suggesting that cohesin is required to stabilize the CPC on the spindle (**Supplementary Fig. 5a**)[21,31].

Markers of late mitotic events enabled us to further explore the spindle defect in cohesin and condensin mutants. Specifically, we monitored localization of Ase1p, the spindle bundling protein that is reported to localize to the spindle midzone only at anaphase onset[32] and Cdc14p, the mitotic exit trigger that regulates the CPC[23]. We found that Ase1p was strictly co-localized to the spindle midzone and the release of Cdc14p from the nucleolus was unaffected in the *smc3-1* and *smc2-8* mutants (**Supplementary Fig. 5b**,**c**). These observations are important because they suggest that cohesin and condensin mutants have initiated mitotic exit[23,32–34] and further suggest that the fishhook spindle observed in these mutants is an anaphase-specific phenotype.

Reduced association of CPC components, Sli15p-GFP and Ipl1p-GFP, with elongated spindles was also observed in double mutants defective in cohesin or condensin components and lacking a functional spindle-assembly checkpoint (*mad1Δ smc3-1* and *mad1Δ smc2-8*) (**Supplementary Fig. 5d**), indicating that CPC mislocalization observed in cohesin/condensin mutants is not due to checkpoint activation[35,36]. Finally, spindle midzone localization of a phosphorylation-deficient CPC mutant (Sli15p-6A-GFP), which binds to the spindle throughout mitosis[23], was delayed in an *smc3-1* mutant resulting in elongated fishhook spindles (**Supplementary Fig. 5e**). This finding is consistent with our checkpoint mutant observations because Sli15p dephosphorylation was previously shown to prevent mitotic checkpoint function during anaphase[37]. Taken together, our results suggest that the observed defect in spindle midzone accumulation and the fishhook phenotype associated with the cohesin and condensin complex is not dependent on activation of the Cdc14p pathway activation but rather is an anaphase-specific event.

Cohesin is concentrated at the pericentromeric region of the yeast chromosomes that overlaps with the spindle midzone[21,31] whereas condensin associates with the kinetochore, chromosomal

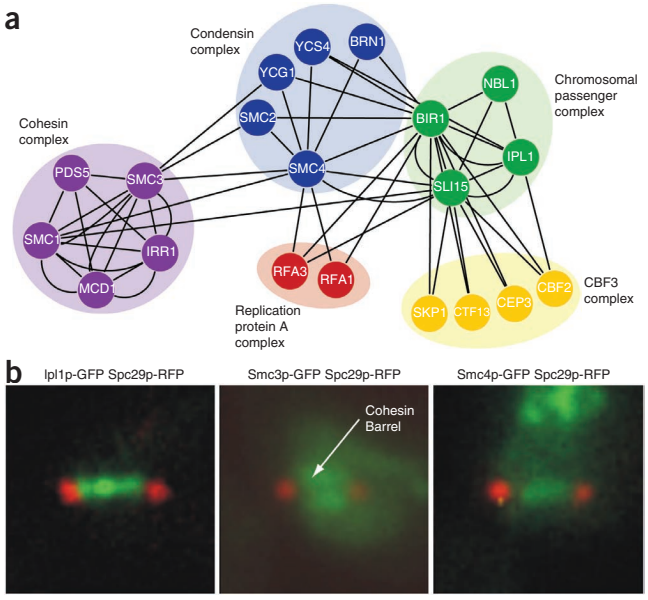

Figure 4 Relationship between cohesin, condensin and chromosomal passenger complexes (CPC). (**a**) Physical interaction network illustrating protein-protein interactions involving cohesin, condensin and CPC complexes. Nodes represent individual proteins and edges represent physical interactions. (**b**) Cohesin, condensin and CPC complex localization. Ipl1p-GFP, Smc3p-GFP and Smc4p-GFP localization was assessed with respect to the spindle pole marker, Spc29p-RFP in a wild-type strain. Fluorescent micrograph images illustrate representative single cells.

© 2011 Nature America, Inc. All rights reserved.

arms and ribosomal DNA (rDNA)[38–40]. Because the CPC plays a major role in controlling spindle disassembly, we decided to test for physical interactions between CPC components, cohesin and condensin. Ipl1p-GFP, Sli15p-GFP, Bir1p-GFP, Smc3p-GFP and Smc4p-GFP were affinity purified from yeast extracts, and then liquid chromatography–tandem mass spectrometry (LC-MS/MS) analysis was carried out. These experiments recapitulated all previously reported interactions (**Fig. 4a** and **Supplementary Table 7**), and they uncovered reproducible interactions between the CPC component, Bir1p-GFP and members of the condensin complex, supporting a direct role for condensin components in stabilizing the CPC (**Fig. 4a**).

To understand the spatial association of these components, we monitored the localization pattern of the CPC, cohesin and condensin complexes in wild-type cells. As reported previously[31], cohesin forms a cylindrical barrel that surrounds Ipl1p (**Fig. 4b** and **Supplementary Fig. 5f**). During metaphase, Ipl1p-GFP localized to the spindle axis and was surrounded by the cohesin barrel, as identified with Smc3p-GFP (**Supplementary Fig. 5f**). As the cells enter anaphase, Ipl1p-GFP was largely restricted within the cohesin-enriched region (**Supplementary Fig. 5f**), suggesting that cohesin restricts the movement of the CPC along the spindle. The condensin component, Smc4p-GFP, displayed a localization pattern similar to that of Ipl1p-GFP along the spindle axis, distinct from the spindle pole body marker, Spc29p-RFP (**Fig. 4b**). Notably, whereas both cohesin and condensin were necessary for the spindle localization of Ipl1p, the localization of cohesin and condensin proteins were unaffected in an *ipl1-2* mutant (**Supplementary Fig. 5g**), suggesting that cohesin and condensin complexes regulate the localization of the CPC and not vice versa. Thus, co-localization of CPC and condensin, within a cohesin barrel, is consistent with the physical interactions observed between the CPC and condensin and between condensin and cohesin.

DISCUSSION

Our ts mutant strain collection contains ts alleles of 497 (~45%) *S. cerevisiae* essential genes. Because each ts allele is linked to a *kanMX* marker, the alleles can be readily used in SGA-based automated genetic analysis, which enables their barcoding for competitive growth assays in pools[17], genetic network mapping[41], high-content screening[21] and a host of other applications. Over ~30% of the essential genes in our collection have multiple alleles (**Supplementary Table 1**), which can be useful for dissecting different roles of multifunctional proteins, such as actin (**Supplementary Fig. 6**). Ultimately, we aim to expand the collection to include a range of ts alleles that cover all domains of essential genes. Indeed, previous efforts to dissect allele-specific interactions involving essential genes have provided significant insight into protein structure and function[42,43].

High content microscopy-based assays of the ts array revealed several new functions for multiple genes (**Fig. 3a**, **Supplementary Fig. 3c** and **Supplementary Table 5**). For example, cellular profiling of our ts collection revealed a connection between the cohesin and condensin complexes and spindle disassembly. Spindle disassembly is a spatiotemporally regulated event such that disassembly of the mitotic spindle occurs only after separation of sister chromatids from the spindle midzone region. Our findings are consistent with a model whereby the CPC decorates the spindle in part through interactions with condensin and cohesin within the vicinity of the centromere[31]. Loss of cohesin/condensin function results in the mislocalization of the CPC, including the Ipl1p kinase that controls spindle disassembly. We speculate that the CPC accesses the spindle midzone only after the cohesin is cleaved, such that cohesin cleavage and clearing of chromosome midzone regions are prerequisites for the mitotic spindle disassembly.

Our collection of ts alleles builds upon a non-overlapping set of strains constructed recently[8]. The combined collections cover the majority of essential genes in the yeast cell and enable numerous systematic approaches for querying the pleiotropic roles of essential genes. For example, we highlighted the use of the collection in chemical-genetic screens for small-molecule suppressors of the ts phenotype, a general screen that may be of particular interest for yeast orthologs of human disease genes because in theory such suppressors may represent therapeutic leads.

Another powerful approach involving ts strains will involve the mapping of genetic interactions by systematic dosage suppression analysis using high-copy libraries, such as the molecular barcoded yeast ORF (MoBY-ORF) library[10] (unpublished data) or the systematic library for comprehensive overexpression analysis[11]. Dosage suppression network interactions are highly abundant and functionally relevant and, even though some of these interactions overlap with protein-protein and negative genetic interactions, most of these suppression edges are unique and offer the potential for expanding our global view of the functional wiring diagram of the cell.

METHODS

Methods and any associated references are available in the online version of the paper at http://www.nature.com/naturebiotechnology/.

Note: Supplementary information is available on the Nature Biotechnology website.

ACKNOWLEDGMENTS

We thank the members of the Boone, Andrews and Bloom laboratory for their input and discussions. We thank S. Biggins (Fred Hutchinson Cancer Research Center) for her insights on cohesin and condensin components. We thank M. Zackrisson (University of Gothenburg) for statistical support. The Sli15-6A-GFP construct was a gift from E. Schiebel (University of Heidelberg) and the Mad1-NLS construct was a gift from R. Wozniak (University of Alberta). We also thank Jennifer Reginold for manual inspection of HCS images. F.J.V. was supported by a postdoctoral fellowship from the Best Foundation. B.A. and C.B. were supported by Genome Canada through the Ontario Genomics Institute as per research agreement 2004-OGI-3-01 and the Canadian Institutes of Health Research (MOP-97939).

AUTHOR CONTRIBUTIONS

Z.L., F.J.V., C.B. and B.A. conceived and designed the experiments. Z.L. and S.B. constructed the ts strains. J.W. and A.B. conducted and analyzed liquid growth profiling experiments. Z.L., F.J.V., F.S.V., J.L., R.M., K.J. and Z.Z. generated and analyzed the HCS data. M.C., A.B., B.V., J.B. and C.L.M. generated and analyzed the data. Z.Y.L. and A.C.G. performed mass spectrometry analyses. Z.L., Z.Y., M.D., J.A.F., C.B., G.G. and C.N. performed the chemical genetic experiments. Z.L., F.J.V., A.S., J.H. and K.B. performed the analysis on cohesin and condensin complexes. H.L., Z.Y., S.B., A.D., G.G., C.N., C.B., M.C., F.S.V., A.D., A.G., Z.Z. and K.B. provided technical support/reagents/materials/analysis tools. Z.L., F.J.V., M.C., B.A. and C.B. wrote the paper.

COMPETING FINANCIAL INTERESTS

The authors declare no competing financial interests.

Published online at http://www.nature.com/nbt/index.html.
Reprints and permissions information is available online at http://www.nature.com/reprints/index.html.

1. Giaever, G. *et al.* Functional profiling of the *Saccharomyces cerevisiae* genome. *Nature* **418**, 387–391 (2002).
2. Kim, D.U. *et al.* Analysis of a genome-wide set of gene deletions in the fission yeast *Schizosaccharomyces pombe*. *Nat. Biotechnol.* **28**, 617–623 (2010).
3. Hughes, T.R. Yeast and drug discovery. *Funct. Integr. Genomics* **2**, 199–211 (2002).
4. Moir, D., Stewart, S.E., Osmond, B.C. & Botstein, D. Cold-sensitive cell-division-cycle mutants of yeast: isolation, properties, and pseudoreversion studies. *Genetics* **100**, 547–563 (1982).
5. Kanemaki, M., Sanchez-Diaz, A., Gambus, A. & Labib, K. Functional proteomic identification of DNA replication proteins by induced proteolysis *in vivo*. *Nature* **423**, 720–724 (2003).
6. Mnaimneh, S. *et al.* Exploration of essential gene functions via titratable promoter alleles. *Cell* **118**, 31–44 (2004).

© 2011 Nature America, Inc. All rights reserved.

7. Schuldiner, M. *et al.* Exploration of the function and organization of the yeast early secretory pathway through an epistatic miniarray profile. *Cell* **123**, 507–519 (2005).
8. Ben-Aroya, S. *et al.* Toward a comprehensive temperature-sensitive mutant repository of the essential genes of *Saccharomyces cerevisiae*. *Mol. Cell* **30**, 248–258 (2008).
9. Brachmann, C.B. *et al.* Designer deletion strains derived from *Saccharomyces cerevisiae* S288C: a useful set of strains and plasmids for PCR-mediated gene disruption and other applications. *Yeast* **14**, 115–132 (1998).
10. Ho, C.H. *et al.* A molecular barcoded yeast ORF library enables mode-of-action analysis of bioactive compounds. *Nat. Biotechnol.* **27**, 369–377 (2009).
11. Jones, G.M. *et al.* A systematic library for comprehensive overexpression screens in *Saccharomyces cerevisiae*. *Nat. Methods* **5**, 239–241 (2008).
12. Giaever, G. *et al.* Chemogenomic profiling: identifying the functional interactions of small molecules in yeast. *Proc. Natl. Acad. Sci. USA* **101**, 793–798 (2004).
13. Hillenmeyer, M.E. *et al.* The chemical genomic portrait of yeast: uncovering a phenotype for all genes. *Science* **320**, 362–365 (2008).
14. Shoemaker, D.D., Lashkari, D.A., Morris, D., Mittmann, M. & Davis, R.W. Quantitative phenotypic analysis of yeast deletion mutants using a highly parallel molecular bar-coding strategy. *Nat. Genet.* **14**, 450–456 (1996).
15. Smith, A.M. *et al.* Quantitative phenotyping via deep barcode sequencing. *Genome Res.* **19**, 1836–1842 (2009).
16. Pierce, S.E., Davis, R.W., Nislow, C. & Giaever, G. Genome-wide analysis of barcoded *Saccharomyces cerevisiae* gene-deletion mutants in pooled cultures. *Nat. Protoc.* **2**, 2958–2974 (2007).
17. Yan, Z. *et al.* Yeast Barcoders: a chemogenomic application of a universal donor-strain collection carrying bar-code identifiers. *Nat. Methods* **5**, 719–725 (2008).
18. Baxter, A. *et al.* Squalestatin 1, a potent inhibitor of squalene synthase, which lowers serum cholesterol *in vivo*. *J. Biol. Chem.* **267**, 11705–11708 (1992).
19. Bergstrom, J.D. *et al.* Zaragozic acids: a family of fungal metabolites that are picomolar competitive inhibitors of squalene synthase. *Proc. Natl. Acad. Sci. USA* **90**, 80–84 (1993).
20. Charlton-Menys, V. & Durrington, P.N. Human cholesterol metabolism and therapeutic molecules. *Exp. Physiol.* **93**, 27–42 (2008).
21. Vizeacoumar, F.J. *et al.* Integrating high-throughput genetic interaction mapping and high-content screening to explore yeast spindle morphogenesis. *J. Cell Biol.* **188**, 69–81 (2010).
22. Buvelot, S., Tatsutani, S.Y., Vermaak, D. & Biggins, S. The budding yeast Ipl1/Aurora protein kinase regulates mitotic spindle disassembly. *J. Cell Biol.* **160**, 329–339 (2003).
23. Pereira, G. & Schiebel, E. Separase regulates INCENP-Aurora B anaphase spindle function through Cdc14. *Science* **302**, 2120–2124 (2003).
24. Ruchaud, S., Carmena, M. & Earnshaw, W.C. The chromosomal passenger complex: one for all and all for one. *Cell* **131**, 230–231 (2007).
25. Sullivan, M., Lehane, C. & Uhlmann, F. Orchestrating anaphase and mitotic exit: separase cleavage and localization of Slk19. *Nat. Cell Biol.* **3**, 771–777 (2001).
26. Zeng, X. *et al.* Slk19p is a centromere protein that functions to stabilize mitotic spindles. *J. Cell Biol.* **146**, 415–425 (1999).
27. Huang, C.E., Milutinovich, M. & Koshland, D. Rings, bracelet or snaps: fashionable alternatives for Smc complexes. *Phil. Trans. R. Soc. Lond. B* **360**, 537–542 (2005).
28. Nasmyth, K. & Haering, C.H. The structure and function of SMC and kleisin complexes. *Annu. Rev. Biochem.* **74**, 595–648 (2005).
29. Guacci, V., Koshland, D. & Strunnikov, A. A direct link between sister chromatid cohesion and chromosome condensation revealed through the analysis of MCD1 in *S. cerevisiae*. *Cell* **91**, 47–57 (1997).
30. Straight, A.F., Sedat, J.W. & Murray, A.W. Time-lapse microscopy reveals unique roles for kinesins during anaphase in budding yeast. *J. Cell Biol.* **143**, 687–694 (1998).
31. Yeh, E. *et al.* Pericentric chromatin is organized into an intramolecular loop in mitosis. *Curr. Biol.* **18**, 81–90 (2008).
32. Khmelinskii, A., Lawrence, C., Roostalu, J. & Schiebel, E. Cdc14-regulated midzone assembly controls anaphase B. *J. Cell Biol.* **177**, 981–993 (2007).
33. Fridman, V., Gerson-Gurwitz, A., Movshovich, N., Kupiec, M. & Gheber, L. Midzone organization restricts interpolar microtubule plus-end dynamics during spindle elongation. *EMBO Rep.* **10**, 387–393 (2009).
34. Schuyler, S.C., Liu, J.Y. & Pellman, D. The molecular function of Ase1p: evidence for a MAP-dependent midzone-specific spindle matrix. Microtubule-associated proteins. *J. Cell Biol.* **160**, 517–528 (2003).
35. Pinsky, B.A. & Biggins, S. The spindle checkpoint: tension versus attachment. *Trends Cell Biol.* **15**, 486–493 (2005).
36. Stern, B.M. & Murray, A.W. Lack of tension at kinetochores activates the spindle checkpoint in budding yeast. *Curr. Biol.* **11**, 1462–1467 (2001).
37. Mirchenko, L. & Uhlmann, F. Sli15(INCENP) Dephosphorylation prevents mitotic checkpoint reengagement due to loss of tension at anaphase onset. *Curr. Biol.* **20**, 1396–1401 (2010).
38. Bachellier-Bassi, S., Gadal, O., Bourout, G. & Nehrbass, U. Cell cycle-dependent kinetochore localization of condensin complex in *Saccharomyces cerevisiae*. *J. Struct. Biol.* **162**, 248–259 (2008).
39. Freeman, L., Aragon-Alcaide, L. & Strunnikov, A. The condensin complex governs chromosome condensation and mitotic transmission of rDNA. *J. Cell Biol.* **149**, 811–824 (2000).
40. Lavoie, B.D., Hogan, E. & Koshland, D. In vivo requirements for rDNA chromosome condensation reveal two cell-cycle-regulated pathways for mitotic chromosome folding. *Genes Dev.* **18**, 76–87 (2004).
41. Costanzo, M. *et al.* The genetic landscape of a cell. *Science* **327**, 425–431 (2010).
42. Amberg, D.C., Basart, E. & Botstein, D. Defining protein interactions with yeast actin *in vivo*. *Nat. Struct. Biol.* **2**, 28–35 (1995).
43. Dreze, M. *et al.* 'Edgetic' perturbation of a *C. elegans* BCL2 ortholog. *Nat. Methods* **6**, 843–849 (2009).
44. Dimster-Denk, D. *et al.* Comprehensive evaluation of isoprenoid biosynthesis regulation in *Saccharomyces cerevisiae* utilizing the Genome Reporter Matrix. *J. Lipid Res.* **40**, 850–860 (1999).
45. Kuranda, K., Francois, J. & Palamarczyk, G. The isoprenoid pathway and transcriptional response to its inhibitors in the yeast *Saccharomyces cerevisiae*. *FEM. Yeast Res.* **10**, 14–27 (2010).
46. Song, J.L., Lyons, C.N., Holleman, S., Oliver, B.G. & White, T.C. Antifungal activity of fluconazole in combination with lovastatin and their effects on gene expression in the ergosterol and prenylation pathways in *Candida albicans*. *Med. Mycol.* **41**, 417–425 (2003).

© 2011 Nature America, Inc. All rights reserved.

ONLINE METHODS

Construction of ts strains. Over 1,300 ts strains covering ~700 essential genes were collected from ~300 different laboratories. Two pairs of primers were used to amplify the ts allele and the *kanMX* cassette (**Supplementary Fig. 1**). Two PCR products (ts allele fragment and *kanMX* cassette) were then co-transformed into BY4741 (*MAT***a** *his3Δ1 leu2Δ0 met15Δ0 ura3Δ0*) and cells were plated on YPD + G418 to select for Kan^R colonies. Transformants were replica-plated twice onto YPD + G418 plates and incubated at 23 °C or 38.5 °C for 1-2 d. Potential ts colonies (lethal/sick at 38.5 °C and healthy at 23 °C) were streaked out on YPD plates, replica-plated onto SC and YPD+G418 plates, and grown for 1-2 d at 23 °C or 38.5 °C. The identified ts colonies (lethal/sick at 38.5 °C) were streaked on six SC plates and at six temperatures (23 °C, 26 °C, 30 °C, 35 °C, 37 °C and 38.5 °C) with a wild-type control (BY4741). Strains that grew well at 23 °C and died or were slow-growing at higher temperatures were frozen down for further confirmation. **Supplementary Table 2** lists the sequences of primers used for constructing the ts strains.

Confirmation of ts strains. Two PCR reactions were carried out to confirm the integration of the ts allele and *kanMX* cassette for the candidate ts strains. One PCR reaction was used to test whether the *kanMX* cassette was linked to the target gene. Another PCR reaction was used to verify that the ts allele and *kanMX* cassette were integrated at the target gene locus (**Supplementary Fig. 1**). The primer sequences for confirmation PCR are listed in **Supplementary Table 2**.

Plasmid complementation. Each ts strain was transformed with the cognate CEN plasmid from the MoBY-ORF library[10] and/or a high-copy plasmid from the yeast genomic tiling collection[11] (Open Biosystem) carrying the wild-type gene, and with a vector control. After growing for 3–5 d at 23 °C, transformants were replica-plated and incubated at 23 °C or at the restrictive temperature for 1–2 d.

Barcoding ts strains. The ts alleles were introduced into the *MAT*α query strain background for synthetic genetic array (SGA) by switching the selectable marker and mating type[47]. The resultant *MAT*α *natMX*-marked ts query strains were arrayed in 96-format on agar plates and mated to an array of Barcoder strains, each carrying a unique *kanMX*-marked barcode cassette[17]. Haploid barcoded ts strains were selected using SGA methodology[47]. The resultant individual barcoded ts strains were then colony-purified and re-arrayed in 96-well-format.

High-resolution liquid growth profiling of the temperature sensitivity of ts alleles. To profile the temperature sensitivity phenotype of the ts alleles, each ts strain ($n = 2$) was micro-cultivated for 3 d at ten temperatures ranging from 22 °C to 40 °C and the change in population density was monitored every 20 min. Specifically, strains were inoculated in 350 µl of SD medium (0.14% yeast nitrogen base, 0.5% ammonium sulfate and 1% succinic acid; 2% (wt/vol) glucose; 0.077% complete supplement mixture (CSM, ForMedium), pH set to 5.8 with NaOH) and precultivated for 48 h at 22 °C. For experimental runs, strains were inoculated to an optical density of 0.03–0.1 in 350 µl of SD medium and cultivated for 72 h in a Bioscreen analyzer C (Growth curves Oy) at the indicated temperature (±0.1 °C) with 10 min preheating time. Optical density (OD) was measured using a wide band (450–580 nm) filter. Plates were subjected to shaking at highest shaking intensity with 60 s of shaking every other minute. OD measurements were taken every 20 min. Strains were run in duplicates on separate plates with four BY4741 replicates in randomized positions on each plate as a reference. Plate layouts were kept unchanged throughout the experimental series.

Three fundamental growth variables, growth lag (time to initiate growth, hours), growth rate (doubling time, hours) and growth efficiency (total density change, ΔOD) were measured to characterize the temperature sensitivity profile of each mutant allele[48,49]. Growth variables of each allele at each temperature were related to the corresponding growth variables of a BY4741 reference strain (BY4741, *his3Δ*; $n = 8$) as ($\log_2$[WT/ts strain]) to provide relative measures of growth. For growth efficiency, this ratio was reversed ($\log_2$[ts strain/WT]). The specific temperature effect of each allele at each temperature was derived by subtracting the relative growth of that allele at 22 °C.

The potential temperature profile similarity of alleles of the same genes was evaluated by comparing the average Pearson correlation coefficient of alleles within the same genes to the average pair-wise Pearson correlation coefficient of alleles of different genes using a two-sample Student's *t*-test with equal variance assumptions. The potential temperature profile similarity of alleles corresponding to genes in the same cellular processes was similarly evaluated by comparing the average Pearson correlation coefficient of alleles within the same cellular processes to the average pairwise Pearson correlation coefficient of alleles of different processes using a two-sample Student's *t*-test with equal variance assumptions, excluding 'within the same gene' relations. Cellular process annotations were obtained from the Saccharomyces Genome Database as "Yeast GO-slim: process" annotations.

Microarray analysis. The homozygous deletion pool containing ~4,700 strains[50] and the ts pool consisting of 440 ts strains plus 162 control strains were prepared, frozen and stored as previously described[16]. Both pools were thawed and diluted in 700 µl of YPD to OD_{600} of 0.06. The homozygous deletion pool and ts pool were separately grown in YPD with zaragozic acid A trisodium salt (ZA, Sigma-Aldrich) or with the solvent DMSO (at 2% final concentration) at 36.5 °C. Cells were collected after five generations using a Robotic Liquid Handling System (http://chemogenomics.med.utoronto.ca/). Both pools were mixed together for genomic DNA preparation, PCR amplification of molecular barcodes and microarray hybridization[16,17]. Data from both pools were then plotted independently. Microarray experiments were repeated three times.

Analysis of growth rates in liquid medium. Wild type (BY4741) and ts strains were grown in YPD for 24 h at 23 °C. The cultures were diluted to OD_{600} of 0.0625 and grown in 100 µl of YPD with either the solvent DMSO or 4 µM of ZA in a 96-well plate. The 96-well plate was constantly shaken in a microplate reader (Tecan, GENios) at 36.5 °C for 20 h and the OD_{600} was read every 15 min. The doubling time of strains was calculated as previously described[51]. The fitness was defined as the ratio of the doubling time of strains grown in the presence of solvent alone (DMSO) relative to ZA treatment. The fitness assays were repeated four times.

Automated image acquisition and analysis. *MAT*α query strains carrying different cellular markers were mated to the ts allele array. *MAT*α haploid ts strains expressing different GFP and/or RFP fusion proteins were isolated using SGA technology[47,52], transferred into liquid selection media and cultured for 1–2 d. Automated imaging and analysis were performed as described previously[21,53,54]. The raw data obtained in both permissive and restrictive temperatures from the HCS experiments are provided in **Supplementary Table 6**.

Confocal microscopy and image quantification. Images were captured using the Quorum WaveFX Spinning Disc Confocal System (Quorum Technologies). The *z*-axis images were converted into a single composite image using the brightest pixel at every position in each of the image planes. This maximum pixel projection technique produced a two-dimensional representation of the GFP fusion proteins within the cell from the three-dimensional data set.

Computational analysis of the HCS data set. To ensure that the identified phenotypes were due to genetic mutations instead of uneven distribution of cell shape, size or cell-cycle stages between mutant and wild-type cell population, the relevant measurements of cellular organelles were scaled into relative morphometric features in comparison with the global cell geometry. For example, for the spindle marker, fiber length was normalized by cell length. The statistical comparison was made based on Wilcoxon Rank Sum test ($P < 0.05$ after Bonferroni multiple testing correction). We further characterized these strains by classifying them as having either no departure from wild-type (0), an enhanced phenotype (+1) or a reduced phenotype (−1) across different features measured. For example, to identify mutants with fishhook spindle, we measured the spindle length in wild-type cells and mutant cells. If a given mutant exhibited elongated spindle compared to wild type it was assigned a score of +1; mutants with spindles shorter than wild type were given a score of −1. If spindle length was unaffected a score of 0 was assigned. Given a predefined functional category, we implemented a genetic algorithm[55] to

© 2011 Nature America, Inc. All rights reserved.
npg

doi:10.1038/nbt.1832

look for an optimal combination of morphological features most predictive of the specified functional category. Support vector machine (SVM) was used to make predictions, and prediction accuracy was assessed by AUC (areas under the receiver operating characteristic curves) on an independent gene set for a blind test. For function prediction across the ts array, SVM ensemble was used to estimate the likelihood of a gene being classified into a given functional category. Briefly, for a given function with its selected features, the entire gene set was split randomly 100 times and each time, a minimal set of genes was used for training and classification was performed on the remaining genes. If a gene was classified more than 50 times into a function, then the corresponding function was assigned to the gene.

Affinity purification and mass spectrometry. Cells expressing GFP- or TAP-tagged proteins (1 liter) were collected at mid-logarithmic phase (A600 = ~0.6), and lysed using glass beads as described[56]. TAP purification was performed as previously described[57]. For GFP affinity purification (AP)-MS, lysates (~150–200 mg protein) were incubated for 2 h at 4 °C with 25 µl GFP-Trap magnetic particles (Chromotek). Beads were then subjected to one rapid wash in 1 ml lysis buffer and one wash in 20 mM Tris pH 8 containing 2 mM $CaCl_2$. On-bead trypsin digestion was performed, followed by LC-MS/MS on a Thermo Finnigan LTQ using the protocols and parameters described previously[57]. Sequence database searching using Mascot 2.2.1 and the *S. cerevisiae* complement of RefSeq release 21 (both forward and reverse entries) was performed, and hits with scores >35 corresponded to a protein false-discovery rate of <4%, determined using a target-decoy strategy[58]. A stringent set of filters were applied to remove likely false positives: (i) all proteins detected in any of three parallel purifications from untagged yeast were removed from the data set; (ii) proteins detected with a frequency of ≥15% across 800 purifications were removed; (iii) only those proteins detected with at least two unique peptides in two biological replicates for any given bait were included in the analysis (their interactions with any of the members of the network are shown).

47. Tong, A.H. & Boone, C. Synthetic genetic array analysis in *Saccharomyces cerevisiae*. *Methods Mol. Biol.* **313**, 171–192 (2006).
48. Warringer, J., Anevski, D., Liu, B. & Blomberg, A. Chemogenetic fingerprinting by analysis of cellular growth dynamics. *BMC Chem. Biol.* **8**, 3 (2008).
49. Warringer, J., Ericson, E., Fernandez, L., Nerman, O. & Blomberg, A. High-resolution yeast phenomics resolves different physiological features in the saline response. *Proc. Natl. Acad. Sci. USA* **100**, 15724–15729 (2003).
50. Lee, W. *et al.* Genome-wide requirements for resistance to functionally distinct DNA-damaging agents. *PLoS Genet.* **1**, e24 (2005).
51. St. Onge, R.P. *et al.* Systematic pathway analysis using high-resolution fitness profiling of combinatorial gene deletions. *Nat. Genet.* **39**, 199–206 (2007).
52. Costanzo, M. & Boone, C. SGAM: an array-based approach for high-resolution genetic mapping in *Saccharomyces cerevisiae*. *Methods Mol. Biol.* **548**, 37–53 (2009).
53. Baryshnikova, A. *et al.* Synthetic genetic array (SGA) analysis in *Saccharomyces cerevisiae* and *Schizosaccharomyces pombe*. *Methods Enzymol.* **470**, 145–179 (2010).
54. Vizeacoumar, F.J., Chong, Y., Boone, C. & Andrews, B.J. A picture is worth a thousand words: genomics to phenomics in the yeast *Saccharomyces cerevisiae*. *FEBS Lett.* **583**, 1656–1661 (2009).
55. Holland, J. *Adaptation in Natural and Artificial Systems: an Introductory Analysis with Applications to Biology, Control, and Artificial Intelligence*. (University of Michigan Press, Ann Arbor, 1975).
56. Gingras, A.C. *et al.* A novel, evolutionarily conserved protein phosphatase complex involved in cisplatin sensitivity. *Mol. Cell. Proteomics* **4**, 1725–1740 (2005).
57. Breitkreutz, A. *et al.* A global protein kinase and phosphatase interaction network in yeast. *Science* **328**, 1043–1046 (2010).
58. Perkins, D.N., Pappin, D.J., Creasy, D.M. & Cottrell, J.S. Probability-based protein identification by searching sequence databases using mass spectrometry data. *Electrophoresis* **20**, 3551–3567 (1999).

© 2011 Nature America, Inc. All rights reserved.